Amplitude Scintillation due to Atmospheric Turbulence for the Deep Space Network Ka-Band Downlink

C. Ho[1] and A. Wheelon[2]

Fast amplitude variations due to atmospheric scintillation are the main concerns for the Deep Space Network (DSN) Ka-band downlink under clear weather conditions. A theoretical study of the amplitude scintillation variances for a finite aperture antenna is presented. Amplitude variances for weak scattering scenarios are examined using turbulence theory to describe atmospheric irregularities. We first apply the Kolmogorov turbulent spectrum to a point receiver for three different turbulent profile models, especially for an exponential model varying with altitude. These analytic solutions then are extended to a receiver with a finite aperture antenna for the three profile models. Smoothing effects of antenna aperture are expressed by gain factors. A group of scaling factor relations is derived to show the dependences of amplitude variances on signal wavelength, antenna size, and elevation angle. Finally, we use these analytic solutions to estimate the scintillation intensity for a DSN Goldstone 34-m receiving station. We find that the (rms) amplitude fluctuation is 0.13 dB at 20-deg elevation angle for an exponential model, while the fluctuation is 0.05 dB at 90 deg. These results will aid us in telecommunication system design and signal-fading prediction. They also provide a theoretical basis for further comparison with other measurements at Ka-band.

I. Introduction

Turbulent irregularities exist in the Earth's lower atmosphere—the troposphere. These mixed air masses act as moving parcels with various sizes, randomly varying in space and time. The parcels of air usually have different temperature, density, humidity, and pressure across their spans. Thus, there are different refractive indexes across them. When radio waves pass through these turbulent cells, their propagation directions and path lengths are altered due to diffraction and scattering. Rapid variations of signals in phase and amplitude thus occur. The wavefront becomes tilted and crinkled in a plane perpendicular to the propagation path. As a result, received signals from all directions and for all instantaneous components are superimposed. This results in the signal being enhanced or diminished

[1] Communications Systems and Research Section.

[2] California Institute of Technology, Trustee, Pasadena, California, pro bono consultant to JPL.

The research described in this publication was carried out by the Jet Propulsion Laboratory, California Institute of Technology, under a contract with the National Aeronautics and Space Administration.

in both phase and amplitude. Random fast fluctuations around the average of field strength are called amplitude scintillations and are the subject of this article.

It is generally known that scintillation intensity (also called fading depth) and signal amplitude increase significantly with increasing signal frequency. This is because the atmosphere has many more turbulent cells with small sizes than larger ones. When the wavelengths of radio signals match the Fresnel lengths of the cells, the scintillation effects become intense. Thus, 32-GHz (Ka-band) signals are expected to have larger fluctuations than those around 8.4 GHz (X-band) and around 2.0 GHz (S-band). The fading depths also increase rapidly with decreasing elevation angles. Because a low elevation path corresponds to a longer atmospheric column, more turbulent cells are included in the propagation path. However, the antenna size tends to reduce scintillation effects since the influence of small turbulent cells is averaged out by large apertures.

Atmospheric scintillations have been extensively studied in both experiments and theories through the last half century [1–4]. A variety of scintillation models have been developed. Turbulence theory becomes the essential in understanding refractive irregularities in the lower atmosphere. The Kolmogorov model is able to explain the most important features of turbulence which cause the perturbation of radio waves. In order to increase the transmission bandwidth, NASA is going to upgrade its Deep Space Network (DSN) downlink frequency to Ka-band. Under fair weather conditions, amplitude variations due to atmospheric scintillation will become the main concern most of the time. This is because fast and deep fadings can cause receiver loss of lock. Under clear weather, at Ka-band the dominant perturbation on receiving signals will come from the scintillation effects. We need to understand how severely this will impact on amplitude variances and how fast the fading can be caused at Ka-band.

In this article, we will revisit turbulence theory to understand how the atmospheric turbulences cause the scintillation for an antenna with finite aperture. Such a detailed investigation for a large antenna at Ka-band has not been done, primarily due to the lack of experiments and applications. For example, if a large antenna aperture can smooth the influence of small turbulent eddies, how much will amplitude variances be reduced? We will start from the random wave equation to develop an analytic solution for a point receiver. Then we will apply the solution to three profile models to describe the height-dependent variation of atmospheric turbulence and then integrate each over a large antenna area. We will apply the Kolmogorov turbulent spectrum into a DSN Ka-band downlink scenario to calculate amplitude variances for the Goldstone receiver. We will re-examine the dependences of amplitude scintillations on frequency, elevation angle, and antenna size for DSN receivers. This study will provide a theoretical basis for any further comparison study with Ka-band measurements. We also extend this study to an exponential profile model, which has not previously been explored.

II. Turbulence Theory

When radio waves pass through the turbulent atmospheric media, the instability of the electric field amplitude is affected by the medium's dielectric constant variance (assuming that the atmosphere has a homogeneous composition, but inhomogeneous temperature and pressure). The relation can be found through solving the following random wave equation:

$$\nabla^2 E + k^2 \big[1 + \delta\varepsilon(r,t)\big] E = 0 \tag{1}$$

This results from Maxwell's equations for the electromagnetic field [1, Section 2.1, pp. 6–10]. Using the Rytov approximation to solve this equation for a small $\delta\varepsilon$ perturbation in the dielectric constant ε, the electric field strength expression becomes [2, Section 2.2, p. 14–19]

$$E(R) = E_0(R) \exp\left[-k^2 \int d^3 r \delta\varepsilon(r) A(R,r)\right] \tag{2}$$

where

$$A(R,r) = \Re\left[G(R,r)\frac{E_0(r)}{E_0(R)}\right] \tag{3}$$

is the real part of the Green function $G(R,r)$ and the ratio of electric fields. We emphasize the natural logarithmic of the amplitude fluctuation:

$$\chi = \ln\left(\frac{E}{E_0}\right)$$

Fluctuations of the field strength ΔE are small compared to E_0 since microwave propagation is described as weak scattering:

$$\chi = \ln\left(\frac{E_0 + \Delta E}{E_0}\right) = \ln\left(1 + \frac{\Delta E}{E_0}\right) \approx \frac{\Delta E}{E_0} < 1 \tag{4}$$

Thus, from Eq. (2),

$$\chi = -k^2 \int d^3 r \delta\varepsilon(r) A(R,r) < 1 \text{ (Np)} \tag{5}$$

If converting χ into decibel units, we have utilized the following relationships:

$$\chi(\text{dB}) = (10 \log_{10} e)\chi(\text{Np}) = 4.34\chi(\text{Np}) \tag{6}$$

$$\left\langle \chi^2 \right\rangle (\text{dB})^2 = (10 \log_{10} e)^2 \left\langle \chi^2 \right\rangle (\text{Np})^2 = 18.84 \left\langle \chi^2 \right\rangle (\text{Np})^2 \tag{7}$$

Because the amplitude fluctuations are referred to their mean value, the ensemble average (represented by an angle bracket) of the amplitude fluctuation vanishes:

$$\langle \chi \rangle = 0 \tag{8}$$

Its mean-square value is not zero, and we can use Eq. (5) to describe the scintillation intensity:

$$\left\langle \chi^2 \right\rangle = k^4 \int d^3 r \int d^3 r' A(R,r) A'(R,r') \left\langle \delta\varepsilon(r,t) \delta\varepsilon(r',t) \right\rangle \ (\text{Np})^2 \tag{9}$$

Because $\varepsilon = n^2$, we can write $\delta\varepsilon = 2n_0\delta n$. When $n_0 = 1$, this becomes $\delta\varepsilon = 2\delta n$, and

$$\left\langle \delta\varepsilon(r,t) \delta\varepsilon(r',t) \right\rangle = 4 \left\langle \delta n(r,t) \delta n(r',t) \right\rangle \tag{10}$$

We know that, in the $r \longleftrightarrow \kappa$ domain [1, Section 2.2.5, pp. 21–23], a three-dimensional Fourier transform connects the spatial covariance of refractive index fluctuations $B_n(r)$ and the wavenumber spectrum of irregularities $\Phi_n(\kappa)$:

$$B_n(\mathbf{r}, \mathbf{r}') = \langle \delta n(r,t) \delta n(r',t) \rangle = \int d^3\kappa \Phi_n(\kappa) \exp\left[i\kappa \cdot (\mathbf{r} - \mathbf{r}') \right] \tag{11}$$

The refractive-index structure function is defined as

$$\mathcal{D}_n(\boldsymbol{\rho}) = \left\langle \left[\delta n(\mathbf{r},t) - \delta n(\mathbf{r}+\boldsymbol{\rho},t) \right]^2 \right\rangle \tag{12}$$

and is often approximated by the following approximation due to Kolmogorov:

$$\mathcal{D}_n(\boldsymbol{\rho}) = C_n^2 \left| \boldsymbol{\rho} \right|^{2/3} \tag{13}$$

where C_n^2 is the refractive-index structure constant and $\boldsymbol{\rho}$ is the spatial difference between two points $\mathbf{r}$ and $\mathbf{r}'$. Previous studies usually have assumed a uniform atmosphere so that C_n^2 is a constant independent of altitude. In this article, we will consider three different altitude profiles of C_n^2 so as to better characterize the real atmosphere. Based on the 2/3 power law on the spatial separation, the wavenumber spectrum of irregularities, $\Phi_n(\kappa)$ for the Kolmogorov refractivity model is expressed as

$$\Phi_n(\kappa, z) = 0.033 C_n^2(z) \kappa^{-(11/3)}, \quad 0 < \kappa < \infty \tag{14}$$

III. Amplitude Variance for a Point Receiver

Consider the vertically downward propagating microwave shown in Fig. 1. After encountering a turbulent eddy, the signal will be diffracted with a small angle θ. In this article, we consider only weak forward scattering. This means that $\theta = \lambda / l \ll 1$, where λ is the wavelength of the radio signal ($\sim$0.01 m) and l is the size of the turbulent cell. Notice that the first Fresnel length is given by $f_L = \sqrt{\lambda z}$. The wavelength of the signal is much less than the size of the turbulent eddies. Because $\theta \ll 1$ (about 1 mrad), and $r \ll z$ in Fig. 1, the downcoming wave stays quite close to the vertical axis. This condition is called the paraxial approximation. The coordinates used in this article are shown in Fig. 2.

For an overhead source, we use the cylindrical coordinates identified in the figure with the point receiver placed at the origin, $R = 0$:

$$E(r) = E_0 \exp(-ikz) \tag{15}$$

$$E(R) = E_0 \tag{16}$$

$$G(R,r) = \frac{1}{4\pi\rho} \exp(ik\rho) \tag{17}$$

where $\rho = \sqrt{z^2 + r^2}$. Both displacement vector ($\boldsymbol{\rho}$) and turbulent wavenumber vector ($\boldsymbol{\kappa}$) in cylindrical coordinates are expressed as

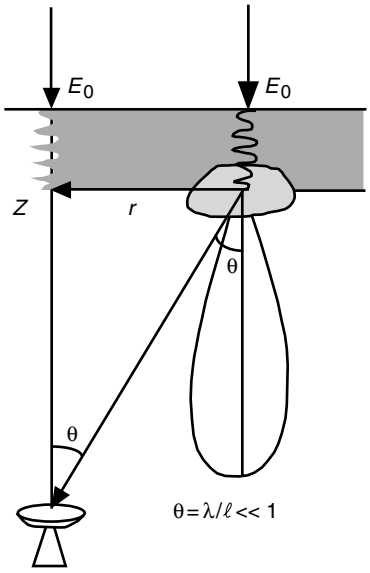

Fig. 1. Geometry showing how a microwave passing through a turbulent refractivity eddy is scattered to the receiver.

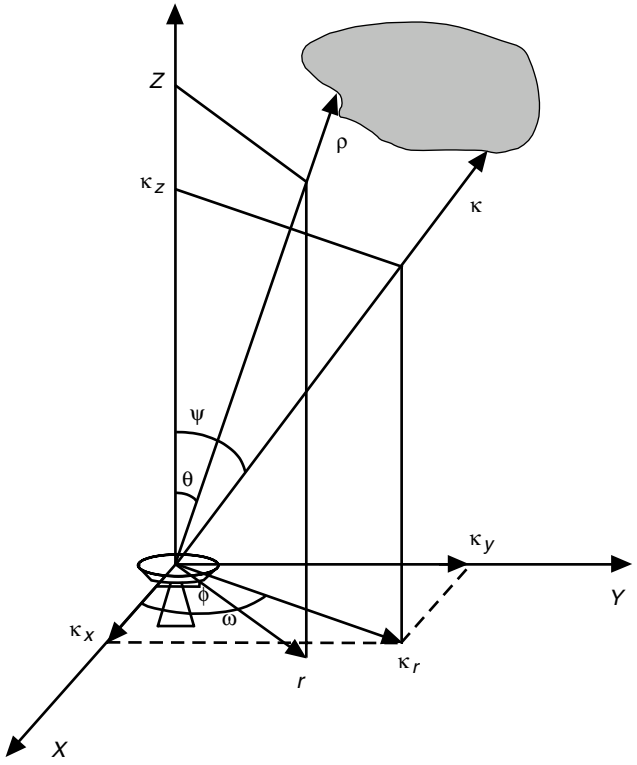

Fig. 2. Coordinate systems describing the displacement vector ρ and the turbulent wavenumber vector κ.

$$\boldsymbol{\rho} = z\boldsymbol{i}_z + r\cos\phi\boldsymbol{i}_x + r\sin\phi\boldsymbol{i}_y \tag{18}$$

$$\boldsymbol{\kappa} = \kappa_z\boldsymbol{i}_z + \kappa_r\cos\omega\boldsymbol{i}_x + \kappa_r\sin\omega\boldsymbol{i}_y \tag{19}$$

Thus, for the amplitude weighting function introduced in Eq. (5), we have

$$A(R,r) = \Re\left[\frac{\exp\left(ik\sqrt{z^2+r^2}\right)}{4\pi\sqrt{z^2+r^2}}\frac{E_0\exp(-ikz)}{E_0}\right] \tag{20}$$

In order to get an analytic solution and in view of the small-angle scattering indicated by Fig. 1, we can expand the square-root distance as follows:

$$\sqrt{z^2+r^2} = z\sqrt{1+\frac{r^2}{z^2}} \approx z + \frac{r^2}{2z}$$

In the numerator of Eq. (20), we must keep both terms but need only the first in the denominator. The amplitude weighting function thus becomes

$$A(R,r) = \Re\left[\frac{\exp\left(ikz + ik\dfrac{r^2}{2z}\right)}{4\pi z}\exp(-ikz)\right]$$

or

$$A(R,r) = \frac{1}{4\pi z}\cos\left(k\frac{r^2}{2z}\right) \tag{21}$$

With this simplified expression, from Eqs. (9) and (10), we can write the variance of logarithmic amplitude fluctuations as

$$\begin{aligned}\left\langle\chi^2\right\rangle = \frac{k^4}{4\pi^2}\int_0^\infty\frac{dz_1}{z_1}\int_0^{2\pi}d\phi_1\int_0^\infty r_1dr_1\cos\left(\frac{kr_1^2}{2z_1}\right)\int_0^\infty\frac{dz_2}{z_2}\\ \times\int_0^{2\pi}d\phi_2\int_0^\infty r_2dr_2\cos\left(\frac{kr_2^2}{2z_2}\right)\left\langle\delta n(\boldsymbol{\rho}_1)\delta n(\boldsymbol{\rho}_2)\right\rangle\end{aligned} \tag{22}$$

In spherical wavenumber coordinates, the spatial covariance of refractive index fluctuations can be expressed as follows:

$$\begin{aligned}\left\langle\delta n(\boldsymbol{\rho}_1)\delta n(\boldsymbol{\rho}_2)\right\rangle &= \int d^3\kappa\Phi_n\left(\kappa,\frac{z_1+z_2}{2}\right)\exp[i\kappa\cdot|\boldsymbol{\rho}_1-\boldsymbol{\rho}_2|]\\ &= \int_0^\infty\kappa^2d\kappa\int_0^\pi d\psi\sin\psi\Phi_n\left(\kappa,\frac{z_1+z_2}{2}\right)\int_0^{2\pi}d\omega\\ &\quad\times\exp\left\{i\left[z_1\kappa\cos\psi + r_1\kappa\sin\psi\cos(\phi_1-\omega)\right] - i\left[z_1\kappa\cos\psi + r_1\kappa\cos\psi\cos(\phi_2-\omega)\right]\right\}\end{aligned} \tag{23}$$

where we have allowed the turbulent spectrum to vary with wavenumber and the average height of the irregularities. Thus,

$$\langle \chi^2 \rangle = \frac{k^4}{4\pi^2} \int_0^\infty \frac{dz_1}{z_1} \int_0^\infty \frac{dz_2}{z_2} \int_0^\infty r_1 dr_1 \int_0^\infty r_2 dr_2 \int_0^\infty \kappa^2 d\kappa \int_0^\pi d\psi \sin\psi \Phi_n \left(\kappa, \frac{z_1+z_2}{2}\right)$$

$$\times \cos\left(\frac{kr_1^2}{2z_1}\right) \exp(iz_1\kappa\cos\psi) \cos\left(\frac{kr_2^2}{2z_2}\right) \exp(-iz_2\kappa\cos\psi) \int_0^{2\pi} d\omega$$

$$\times \int_0^{2\pi} \exp\left[r_1\kappa\sin\psi\cos(\phi_1-\omega)\right] d\phi_1 \int_0^{2\pi} \exp\left[r_2\kappa\sin\psi\cos(\phi_2-\omega)\right] d\phi_2 \tag{24}$$

Using the integral relation Eq. (A-1) in Appendix A to integrate $d\phi_1 d\phi_2 d\omega$, we can reduce this as follows:

$$\langle \chi^2 \rangle = 2\pi k^4 \int_0^\infty \kappa^2 d\kappa \int_0^\pi d\psi \sin\psi$$

$$\times \int_0^\infty \frac{dz_1}{z_1} \int_0^\infty \frac{dz_2}{z_2} \exp\left[i(z_1-z_2)\kappa\cos\psi\right] \Phi_n \left(\kappa, \frac{z_1+z_2}{2}\right)$$

$$\times \int_0^\infty r_1 dr_1 \cos\left(\frac{kr_1^2}{2z_1}\right) J_0(r_1\kappa\sin\psi) \times \int_0^\infty r_2 dr_2 \cos\left(\frac{kr_2^2}{2z_2}\right) J_0(r_2\kappa\sin\psi) \tag{25}$$

Using the relation Eq. (A-2) in Appendix A, we can perform the radial integrations to find

$$\langle \chi^2 \rangle = 2\pi k^2 \int_0^\infty \kappa^2 d\kappa \int_0^\pi d\psi \sin\psi \int_0^\infty dz_1 \int_0^\infty dz_2 \exp\left[i\kappa\cos\psi(z_1-z_2)\right]$$

$$\times \sin\left(\frac{z_1\kappa^2\sin^2\psi}{2k}\right) \sin\left(\frac{z_2\kappa^2\sin^2\psi}{2k}\right) \Phi_n \left(\kappa, \frac{z_1+z_2}{2}\right) \tag{26}$$

The variation of the exponential term is very rapid and destructive unless the values of z_1 and z_2 are very close to each other. This lets us approximate the double integral as follows:

$$\int_0^\infty dz_1 \int_0^\infty dz_2 \exp\left[i\kappa\cos\psi(z_1-z_2)\right] F(z_1,z_2) \simeq 2\pi\delta(\kappa\cos\psi) F(z,z) \tag{27}$$

where

$$z = \frac{z_1+z_2}{2}$$

where we exploit the Delta function relations provided in Eqs. (A-5) through (A-7) in Appendix A to write

$$\left\langle \chi^2 \right\rangle = 4\pi^2 k^2 \int_0^\infty \kappa d\kappa \int_0^\pi d\psi \sin\psi \Phi_n(\kappa, z) \int_0^\infty \delta(\cos\psi) \sin^2\left(\frac{z\kappa^2 \sin^2\psi}{2k}\right) dz \tag{28}$$

Since the delta function requires that $\cos\psi = 0$ and $\sin\psi = 1$, we have finally

$$\left\langle \chi^2 \right\rangle = 4\pi^2 k^2 \int_0^\infty \kappa d\kappa \Phi_n(\kappa, z) \int_0^\infty \sin\left(\frac{z\kappa^2}{2k}\right) dz \tag{29}$$

IV. Results for Three Turbulent Profiles

We will apply the Kolmogorov spectrum to describe the turbulent irregularities for a point receiver. In doing so, we consider three profile models to describe the altitude variation of turbulence strength, as represented in the parameter C_n^2. The profile models are (1) uniform slab, (2) thin layer, and (3) exponential. They are illustrated in Fig. 3.

A. Slab Model

In this case, we assume that all atmospheric turbulent eddies are of uniform strength and contained within a limited height, H:

$$C_n^2(z) = C_n^2 \begin{cases} 1 & 0 < z \leq H \\ 0 & H > z \end{cases} \tag{30}$$

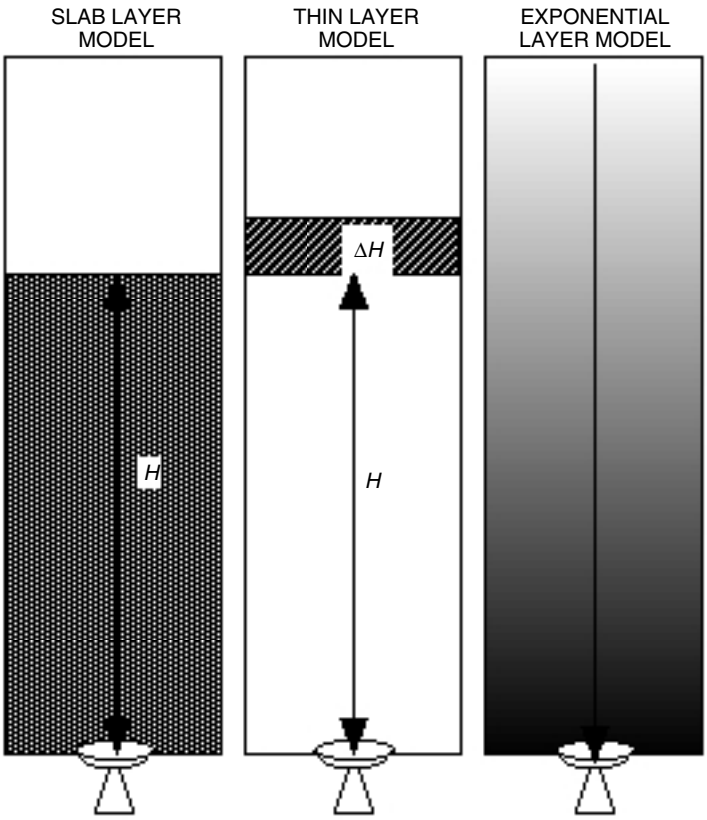

Fig. 3. Three profiles used to describe the level of atmospheric turbulence: (1) slab with uniform density, (2) thin layer with thickness ΔH, and (3) exponential decayed atmosphere.

After applying the Kolmogorov spectrum and slab model into the expression of amplitude variances, Eq. (29), we have

$$\begin{aligned}\left\langle \chi^2 \right\rangle &= 4\pi^2 k^2 \int_0^\infty \kappa d\kappa \int_0^H dz \Phi_n(\kappa, z) \sin\left(\frac{z\kappa^2}{2k}\right) dz \\ &= 2\pi^2 H k^2 \int_0^\infty \kappa d\kappa \, 0.033 \, C_n^2 \kappa^{-(11/3)} \left(1 - \frac{\sin(H\kappa^2/k)}{H\kappa^2/k}\right) \\ &= 0.651 k^2 H C_n^2 \int_0^\infty \frac{d\kappa}{\kappa^{8/3}} \left(1 - \frac{\sin(H\kappa^2/k)}{H\kappa^2/k}\right) \end{aligned} \tag{31}$$

Substituting $\zeta = H\kappa^2/k$, we have the following for the point receiver:

$$\left\langle \chi^2 \right\rangle = 0.326 C_n^2 H^{11/6} k^{7/6} \int_0^\infty \frac{d\zeta}{\zeta^{11/6}} \left(1 - \frac{\sin\zeta}{\zeta}\right) \tag{32}$$

or finally

$$\left\langle \chi^2 \right\rangle = 0.307 C_n^2 H^{11/6} k^{7/6} \ (\text{Np})^2 \tag{33}$$

B. Thin Layer

A thin layer of thickness ΔH often is used to describe a turbulent layer or a cloud layer at a fixed altitude H. This is defined as [4–6]

$$C_n^2(z) = C_n^2 \begin{cases} 1 & H < z < H + \Delta H \\ 0 & \text{otherwise} \end{cases} \tag{34}$$

When $\Delta H << H$, we have

$$\begin{aligned}\left\langle \chi^2 \right\rangle &= 4\pi^2 k^2 \int_0^\infty \kappa d\kappa \Phi_n(\kappa, z) \int_0^\infty \sin\left(\frac{z\kappa^2}{2k}\right) dz \\ &= 2\pi^2 k^2 \int_0^\infty \kappa d\kappa \Phi_n(\kappa, z) \int_0^\infty \left[1 - \cos\left(\frac{z\kappa^2}{2k}\right)\right] dz \\ &= 0.651 k^2 \Delta H C_n^2 \int_0^\infty \frac{d\kappa}{\kappa^{8/3}} \left[1 - \cos\left(\frac{H\kappa^2}{k}\right)\right] \end{aligned} \tag{35}$$

Using a substitution of $\zeta = H\kappa^2/k$, we have

$$\left\langle \chi^2 \right\rangle = 0.326 C_n^2 \Delta H H^{5/6} k^{7/6} \int_0^\infty \frac{d\zeta}{\zeta^{11/6}} \left[1 - \cos\zeta\right] = 0.563 C_n^2 \Delta H H^{5/6} k^{7/6} \ (\text{Np})^2 \tag{36}$$

C. Exponential Model

In the third case, we assume that atmospheric turbulence level has its maximum value at the Earth's surface and decreases exponentially with altitude. It is defined as

$$C_n^2(z) = C_n^2(0) \exp\left(-\frac{z}{H}\right) \tag{37}$$

where H is the scale height. Thus,

$$\Phi_n(\kappa, z) = 0.033\kappa^{-(11/3)} C_n^2(0) \exp\left(-\frac{z}{H}\right) \tag{38}$$

We have

$$\begin{aligned}
\left\langle \chi^2 \right\rangle &= 4\pi^2 k^2 \int_0^\infty \kappa d\kappa \, 0.033 \, \kappa^{-(11/3)} C_n^2(0) \int_0^\infty \exp\left(-\frac{z}{H}\right) \sin\left(\frac{z\kappa^2}{2k}\right) dz \\
&= 0.651 k^2 C_n^2(0) \int_0^\infty \frac{d\kappa}{\kappa^{8/3}} \int_0^\infty \exp\left(-\frac{z}{H}\right) \left[1 - \cos\left(\frac{z\kappa^2}{2k}\right)\right] dz \\
&= 0.651 k^2 C_n^2(0) H \int_0^\infty \frac{d\kappa}{\kappa^{8/3}} \frac{\left(\frac{H\kappa^2}{k}\right)^2}{1 + \left(\frac{H\kappa^2}{k}\right)^2}
\end{aligned} \tag{39}$$

Using a substitution of $\zeta = H\kappa^2/k$, we have

$$\left\langle \chi^2 \right\rangle = 0.326 k^{7/6} C_n^2(0) H^{11/6} \int_0^\infty \frac{d\zeta}{\zeta^{11/6}} \frac{\zeta^2}{1+\zeta^2} = 0.530 k^{7/6} C_n^2(0) H^{11/6} \tag{40}$$

Using the integral result, Eq. (A-10), we have

$$\left\langle \chi^2 \right\rangle = 0.530 k^{7/6} C_n^2(0) H \tag{41}$$

for an exponential model.

D. Oblique Paths

For an oblique path with elevation angle ϑ, we should replace H with $H \csc\vartheta$. Amplitude variances for three profile models with a point receiver become

$$\left\langle \chi^2 \right\rangle = 0.307 C_n^2 k^{7/6} H^{11/6} (\csc\vartheta)^{11/6} \quad (\text{Np})^2 \quad \text{for a slab model} \tag{42}$$

$$\left\langle \chi^2 \right\rangle = 0.563 C_n^2 k^{7/6} \Delta H H^{5/6} (\csc\vartheta)^{11/6} \quad (\text{Np})^2 \quad \text{for a thin layer model} \tag{43}$$

$$\left\langle \chi^2 \right\rangle = 0.530 C_{n_0}^2 k^{7/6} H^{11/6} (\csc\vartheta)^{11/6} \quad (\text{Np})^2 \quad \text{for an exponential model} \tag{44}$$

V. Antenna Aperture-Averaging Effects

For a receiving antenna with effective antenna radius a_r, amplitude variance is an integration over the entire antenna area [2,4,7,8]:

$$\overline{\langle\chi^2\rangle} = \frac{1}{A^2}\iint_A d^2\sigma_1 \iint_A d^2\sigma_2 \,\langle\chi(\rho_1)\chi(\rho_2)\rangle = \frac{1}{\pi^2 a_r^2}\int_0^{a_r}\rho_1 d\rho_1 \int_0^{2\pi} d\phi_1$$

$$\times \int^{a_r}\rho_2 d\rho_2 \int_0^{2\pi} d\phi_2 \,\langle\chi(\rho_1,\phi_1)\chi(\rho_2,\phi_2)\rangle \tag{45}$$

Figure 4 shows two surface elements, σ_1 and σ_2, with a scalar distance $|\boldsymbol{\sigma}_1 - \boldsymbol{\sigma}_2|$ on the receiving aperture. Spatial cross-correlation between two surface elements will generate a joint term $J_0(\kappa\,|\boldsymbol{\sigma}_1 - \boldsymbol{\sigma}_2|)$ for the two-dimensional integration below.

Based on the spatial covariance for a plane wave shown in Appendix B, the joint amplitude variances from two adjacent elements within an antenna dish can be expressed as

$$\langle\chi(\sigma_1)\chi(\sigma_2)\rangle = 4\pi^2 k^2 \int_0^{\infty}\kappa d\kappa \Phi_n(\kappa) J_0\left(\kappa\,|\boldsymbol{\sigma}_1 - \boldsymbol{\sigma}_2|\right)\int_0^H \sin^2\left(\frac{z\kappa^2}{2k}\right)dz$$

$$= 2\pi^2 k^2 \int_0^{\infty}\kappa d\kappa \Phi_n(\kappa) J_0\left(\kappa\,|\boldsymbol{\sigma}_1 - \boldsymbol{\sigma}_2|\right)\int_0^H \left[1-\cos\left(\frac{z\kappa^2}{k}\right)\right]dz$$

$$= 2\pi^2 H k^2 \int_0^{\infty}\kappa d\kappa \Phi_n(\kappa) J_0\left(\kappa\,|\boldsymbol{\sigma}_1 - \boldsymbol{\sigma}_2|\right)\left[1-\frac{\sin(H\kappa^2/k)}{H\kappa^2/k}\right] \tag{46}$$

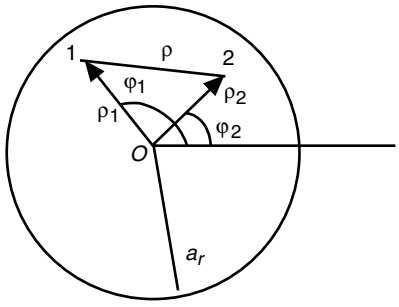

Fig. 4. A two-dimensional integration is performed over a circular dish antenna with finite radius a_r. Two surface elements show how they are cross-correlated, and the fluctuations received by surface elements are spatially averaged out due to the reduced gain factor for a large aperture antenna.

The spatial average over the entire antenna surface is

$$\begin{aligned}\overline{\langle\chi^2\rangle} &= \frac{2Hk^2}{a_r^2}\int_0^{a_r}\rho_1 d\rho_1\int_0^{2\pi}d\phi_1\int_0^{a_r}\rho_2 d\rho_2\int_0^{2\pi}d\phi_2 \\ &\quad\times\int_0^{\infty}\kappa d\kappa\Phi_n(\kappa)J_0\left(\kappa\left|\boldsymbol{\rho}_1-\boldsymbol{\rho}_2\right|\right)\left[1-\frac{\sin(H\kappa^2/k)}{H\kappa^2/k}\right] \\ &= \frac{2Hk^2}{a_r^2}\int_0^{\infty}\kappa d\kappa\Phi_n(\kappa)\left[1-\frac{\sin(H\kappa^2/k)}{H\kappa^2/k}\right]\int_0^{a_r}\rho_1 d\rho_1\int_0^{2\pi}d\phi_1\int_0^{a_r}\rho_2 d\rho_2 \\ &\quad\times\int_0^{2\pi}d\phi_2 J_0\left(\kappa\sqrt{\rho_1^2+\rho_2^2-2\rho_1\rho_1\cos(\phi_2-\phi_1)}\right) \end{aligned} \tag{47}$$

The addition theorem for Bessel functions separates the integrations as shown in Eq. (A-3). The angular integrations result in only one term ($n = 0$) in the series left. Using the expression shown in Eq. (A-4), we have

$$\frac{1}{\pi^2 a_r^4}\int_0^{a_r}\rho_1 d\rho_1\int_0^{2\pi}d\phi_1\int_0^{a_r}\rho_2 d\rho_2\int_0^{2\pi}d\phi_2 J_0\left(\kappa\sqrt{\rho_1^2+\rho_2^2-2\rho_1\rho_1\cos(\phi_2-\phi_1)}\right)=\left[\frac{2J_1(\kappa a_r)}{\kappa a_r}\right]^2 \tag{48}$$

Thus,

$$\overline{\langle\chi^2\rangle} = 4\pi^2k^2\int_0^{\infty}\kappa d\kappa\int_0^{H}dz\Phi_n(\kappa,z)\sin^2\left(\frac{z\kappa^2}{2k}\right)\left[\frac{2J_1(\kappa a_r)}{\kappa a_r}\right]^2 \tag{49}$$

or

$$\overline{\langle\chi^2\rangle} = 2\pi^2k^2\int_0^{\infty}\kappa d\kappa\int_0^{H}dz\Phi_n(\kappa,z)\left[1-\cos\left(\frac{z\kappa^2}{k}\right)\right]\left[\frac{2J_1(\kappa a_r)}{\kappa a_r}\right]^2 \tag{50}$$

where the term $\left(2J_1(\kappa a_r)/\kappa a_r\right)^2$ is the aperture-averaging wavenumber weighting function (or the Airy function). It acts like a lowpass filter and eliminates the contribution from those turbulence eddies smaller than the radius of the receiver, a_r.

A. Slab Model

Applying the Kolmogorov spectrum with a slab profile model of thickness H, we have

$$\begin{aligned}\overline{\langle\chi^2\rangle} &= 2\pi^2Hk^2\int_0^{\infty}\kappa d\kappa 0.033C_n^2\kappa^{-(11/3)}\left(1-\frac{\sin(H\kappa^2/k)}{H\kappa^2/k}\right)\left[\frac{2J_1(\kappa a_r)}{\kappa a_r}\right]^2 \\ &= 0.651k^2HC_n^2\int_0^{\infty}\frac{d\kappa}{\kappa^{8/3}}\left(1-\frac{\sin(H\kappa^2/k)}{H\kappa^2/k}\right)\left[\frac{2J_1(\kappa a_r)}{\kappa a_r}\right]^2 \\ &= 0.307C_n^2H^{11/6}k^{7/6}G_1\left(a_r\sqrt{\frac{2\pi}{H\lambda}}\right)\quad(\text{Np})^2 \end{aligned} \tag{51}$$

where $a_r\sqrt{2\pi/H\lambda}$ is the ratio of antenna size, a_r, over the first Fresnel zone size, $\sqrt{H\lambda/2\pi}$. After we use substitutions of $\eta = a_r\sqrt{2\pi/H\lambda} = a_r\sqrt{k/H}$, $\zeta = H\kappa^2/k$, the gain factor can be defined as

$$G_1(\eta) = 1.060 \int_0^\infty \frac{d\zeta}{\zeta^{11/6}} \left(1 - \frac{\sin\zeta}{\zeta}\right) \left[\frac{2J_1\left(\eta\sqrt{\zeta}\right)}{\eta\sqrt{\zeta}}\right]^2 \tag{52}$$

The integral $G_1(\eta)$ cannot be solved analytically unless some approximations or simplifications are made. However, we can solve it by the numerical integration. The numerical solution for the gain factor is shown in Fig. 5 as a function of the ratio (η) of antenna size over the first Fresnel zone size. If we normalize Eq. (51) by the point receiver solution, Eq. (33), we will have

$$\frac{\overline{\langle\chi^2(a_r)\rangle}}{\langle\chi^2(0)\rangle} = G_1(\eta) \tag{53}$$

The ratio of amplitude fluctuations between a finite aperture receiver and a point receiver is its gain factor. As expected, the antenna aperture plays a role in smoothing the amplitude fluctuations, because the gain factor, $G(\eta)$, is always less than 1 and also rapidly decreases with increasing aperture size. Thus, the amplitude variations for a large antenna are always less than those for a point antenna.

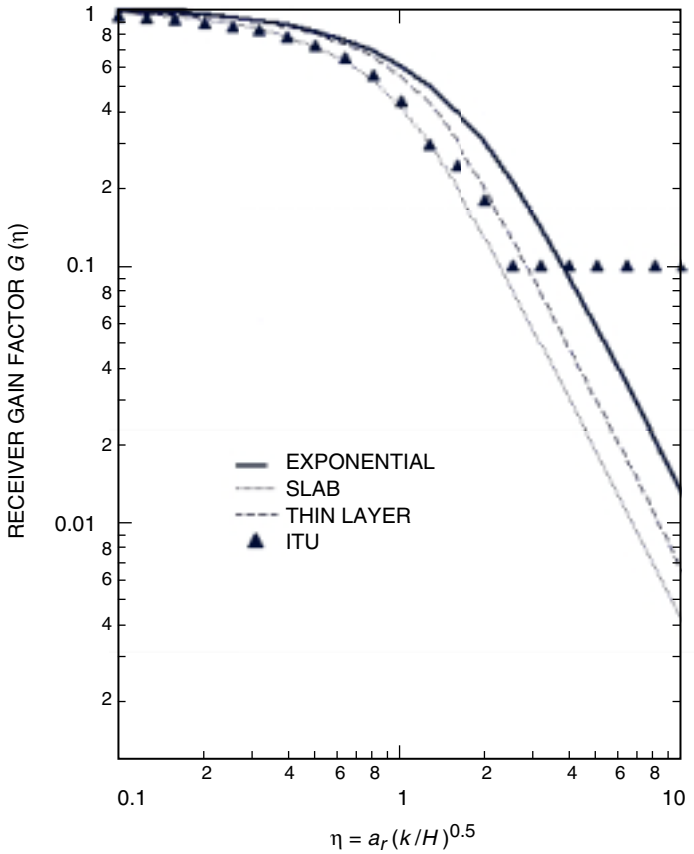

Fig. 5. Gain factors for three types of turbulent layer models as a function of antenna size. The ITU model is also shown with a cutoff at $G(\eta) = 0.1$.

B. Thin Layer

Assuming a layer of thickness ΔH at altitude H and also taking $\Delta H << H$, we have

$$\overline{\langle \chi^2 \rangle} = 0.563 C_n^2 \Delta H H^{5/6} k^{7/6} G_2 \left(a_r \sqrt{\frac{2\pi}{H\lambda}} \right) \quad (\text{Np})^2 \tag{54}$$

where

$$G_2(\eta) = 0.578 \int_0^\infty \frac{d\zeta}{\zeta^{11/6}} \left[1 - \cos \zeta \right] \left[\frac{2 J_1 \left(\eta \sqrt{\zeta} \right)}{\eta \sqrt{\zeta}} \right]^2 \tag{55}$$

The gain factor for a thin layer model is plotted in Fig. 5.

C. Exponential Model

Similarly, we have

$$\overline{\langle \chi^2 \rangle} = 0.530 C_{n_0}^2 H^{11/6} k^{7/6} G_3 \left(a_r \sqrt{\frac{2\pi}{H\lambda}} \right) \quad (\text{Np})^2 \tag{56}$$

where

$$G_3(\eta) = 0.615 \int_0^\infty \frac{d\zeta}{\zeta^{11/6}} \frac{\zeta^2}{1+\zeta^2} \left[\frac{2 J_1 \left(\eta \sqrt{\zeta} \right)}{\eta \sqrt{\zeta}} \right]^2 \tag{57}$$

The gain factor for an exponential model is also shown in Fig. 5. As compared with the other two models, the exponential model has the largest effect. We also see that all gain factors go to the unit when $\eta \longrightarrow 0$. The amplitude variance becomes the solution of a point receiver. The gain factor does not depend on either antenna size or Fresnel length alone. It strongly depends on the ratio (η) of antenna size over the first Fresnel length.

D. Comparison with the International Telecommunication Union Model

Crane and Blood[3] generate a piecewise function to express the antenna aperture-averaging gain factor for amplitude scintillation. This function defines the International Telecommunication Union (ITU) model as

$$G(a_r) = \begin{cases} 1.0 - 1.4 \left(a_r / \sqrt{H\lambda} \right) & \text{for } 0 \le a_r / \sqrt{H\lambda} \le 0.5 \\ 0.5 - 0.4 \left(a_r / \sqrt{H\lambda} \right) & \text{for } 0.5 < a_r / \sqrt{H\lambda} \le 1.0 \\ 0.1 & \text{for } 1.0 < a_r / \sqrt{H\lambda} \end{cases} \tag{58}$$

The results for this model are also shown in Fig. 5. We can see that the ITU model fits a slab model very well when $a_r / \sqrt{H\lambda} < 1.4$.

[3] R. K. Crane and D. W. Blood, *Handbook for the Estimation of Microwave Propagation Effects-Link Calculations for Earth-Space Paths*, Tech. Rep. 1, Document P.7376-TR1 (internal document), prepared for NASA Goddard Space Flight Center, Greenbelt, Maryland, June 1979.

VI. Scaling Factors

Based on the above analytical solutions, we can obtain the following amplitude scintillation dependences on the wavelength, antenna size, and elevation angles.

A. Frequency Dependence

Noting the electromagnetic wavenumber is $k = 2\pi/\lambda$, we have for a point receiver

$$\frac{\langle \chi_1^2 \rangle}{\langle \chi_2^2 \rangle} = \left(\frac{k_1}{k_2}\right)^{7/6} = \left(\frac{\lambda_2}{\lambda_1}\right)^{7/6} \approx \left(\frac{f_1}{f_2}\right)^{7/6} \tag{59}$$

when the signal's wavelength and frequency have the relation of $\lambda f = v_g$ and assuming that the wave propagation speed, v_g, is a constant.

For example, relative to X-band (8.4 GHz), the amplitude variance at Ka-band (32 GHz) will increase by a factor of 4.8.

The gain factor for a finite aperture antenna expressed as a function of wavelength is

$$\frac{\left\langle \overline{\chi_1^2(\lambda_1)} \right\rangle}{\left\langle \overline{\chi_2^2(\lambda_2)} \right\rangle} = \left(\frac{\lambda_2}{\lambda_1}\right)^{7/6} \frac{G\left(a_r\sqrt{\frac{2\pi}{H\lambda_1}}\right)}{G\left(a_r\sqrt{\frac{2\pi}{H\lambda_2}}\right)} \tag{60}$$

B. Antenna Size

Normalizing Eqs. (51) through (53) by Eqs. (33), (36), and (41), respectively, we have

$$\frac{\overline{\langle \chi^2(a_r) \rangle}}{\langle \chi^2(0) \rangle} = G\left(a_r\sqrt{\frac{2\pi}{H\lambda}}\right) \tag{61}$$

which also depends on what type of turbulent profile models one chooses.

C. Elevation Angle

From Expressions (42) through (44), we can find

$$\frac{\langle \chi^2(\vartheta_1) \rangle}{\langle \chi^2(\vartheta_2) \rangle} = \left(\frac{\sin\vartheta_2}{\sin\vartheta_1}\right)^{11/6} \quad \text{for} \quad \vartheta \geq 5 \text{ deg} \tag{62}$$

The relation will be broken up at 5 deg and below because of multipath effects at low elevation angles.

VII. DSN Goldstone Receiver

Now we can apply these analytic solutions to a 34-m parabolic dish antenna at the Goldstone DSN site at Ka-band. We will use the following parameters for the Goldstone site calculation [9,10]:

$$C_{n_0}^2 = 0.5 \times 10^{-13} \left(\mathrm{m}^{-(2/3)} \right)$$

$$\lambda = 0.01 \text{ (m)}$$

$$H = 8.0 \times 10^3 \text{ (m)}$$

$$a_r = 34/2 \times 55\% \text{ (m)}$$

Here we have assumed that the dish antenna has a 55 percent efficiency relative to its physical radius. We will show an example of how to calculate the amplitude variations, as follows. From Fig. 6, we can find that, when $\eta = a_r \sqrt{2\pi/\lambda H} = 2.62$, $G_1(\eta) = 0.075$ for a slab model; $G_2(\eta) = 0.12$ for a thin layer model; and $G_3(\eta) = 0.19$ for an exponential model. Thus, when elevation angle $\vartheta = 90$ deg, for an exponential model we have, from Eq. (56),

$$\overline{\langle \chi^2 \rangle} = 0.530 C_{n_0}^2 H^{11/6} k^{7/6} (\sin\vartheta)^{-(11/6)} G_3 \left(a_r \sqrt{\frac{2\pi}{H\lambda}} \right) \quad (\mathrm{Np})^2 \tag{63}$$

$$\left\langle \chi^2 \right\rangle = 1.33 \times 10^{-4} \quad (\mathrm{Np})^2 \tag{64}$$

Its root of mean square (rms), that is, amplitude fluctuation, is

$$\chi_{\mathrm{rms}} = 1.15 \times 10^{-2} \quad (\mathrm{Np})$$

Using Eq. (6) and converting to decibels, we have

$$\chi_{\mathrm{rms}} = 0.05 \quad (\mathrm{dB})$$

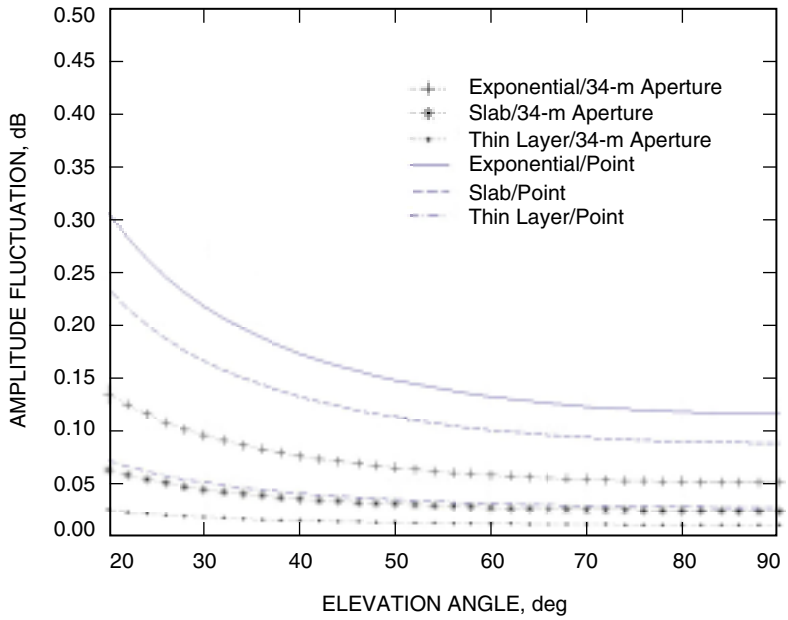

Fig. 6. Elevation-angle dependence of amplitude fluctuation (in decibels) for both a 34-m DSN antenna and a point receiver for three types of atmospheric profile models.

When elevation angle $\vartheta = 20$ deg,

$$\left\langle \chi^2 \right\rangle = 9.51 \times 10^{-4} \quad (\text{Np})^2$$

$$\chi_{\text{rms}} = 3.08 \times 10^{-2} \quad (\text{Np})$$

$$\chi_{\text{rms}} = 0.134 \quad (\text{dB})$$

Figure 6 shows the amplitude fluctuations for elevation angles from 20 deg to 90 deg for three atmospheric turbulent models for a DSN 34-m antenna at Goldstone; the DSN antenna will not operate below the 20-deg elevation angle for Ka-band. For comparison, the amplitude variations for a point receiver also are shown in the figure. To calculate the amplitude fluctuation for a thin layer, we have assumed a 400-m layer thickness. Of the three models, the exponential model has high amplitude variations because of its large gain factor. The ratio of amplitude changes between a receiver with finite radius a_r and a point receiver is

$$\frac{\chi_{\text{rms}}(a_r)}{\chi_{\text{rms}}(0)} = \sqrt{G\left(a_r\sqrt{\frac{2\pi}{H\lambda}}\right)} \tag{65}$$

VIII. Summary

On the basis of the Kolmogorov turbulence theory, we have derived all analytical solutions for the amplitude variances for a finite aperture antenna for the DSN scenario. Through this analytical study, we found that amplitude scintillation is an important factor that cannot be neglected under the clear weather at Ka-band, even for the large antenna used at Goldstone. At low elevation angles, the scintillation intensity remains high. For example, at a 20-deg elevation, amplitude fluctuation can be as much as 0.13 dB for a 34-m DSN antenna for an exponential turbulent model. If these fast fadings are further superimposed on some slow fadings (caused by water vapor density changes), deep fading will definitely cause a problem for the DSN link. Using these fluctuation values, we can further study power spectra and fading rates of the amplitude scintillations [11].

A receiver antenna with finite aperture will have different effects from a point receiver on the scintillation intensity and temporal characteristics. Because the receiver's output is a spatial average of the wavefront fluctuations over the aperture, this results in the observed fluctuations being smaller than those received by a point receiver. We can see that the gain factor for a finite aperture antenna strongly depends on the ratio (η) of antenna size over the first Fresnel zone size. The gain factor also is dependent on what types of atmospheric turbulence profile models we use.

These results should help in system design and fading prediction for Ka-band downlink for a low-margin telecommunication system such as the DSN. It also establishes the theoretical basis for any future experimental comparison at Ka-band. The fading study on atmospheric scintillation also provides us a possible mitigation approach in controlling the uplink power based on predicted amplitude fluctuations.

Acknowledgments

We wish to thank the Program Manager, Julian Breidenthal, for his support in this propagation effect study. We also are indebted to Charles Lee for his reviewing of this article and Bob Crane for his comments and suggestions on this work. The authors are grateful to Kelly Gritton for her help in Bessel function computing, Peter Wheelon for graphic work, and Roger Carlson for his technical editing of this article.

References

[1] A. D. Wheelon, *Electromagnetic Scintillation I. Geometrical Optics*, Cambridge, United Kingdom: Cambridge University Press, 2001.

[2] A. D. Wheelon, *Electromagnetic Scintillation II. Weak Scattering*, Cambridge, United Kingdom: Cambridge University Press, 2003.

[3] V. I. Tatarskii, *The Effects of the Turbulent Atmosphere on Wave Propagation*, National Technical Information Office, U.S. Department of Commerce, Springfield, Virginia, 1971.

[4] J. Haddon and E. Vilar, "Scattering Induced Microwave Scintillations from Clear Air and Rain on Earth Space Paths and the Influence of Antenna Aperture," *IEEE Transactions on Antennas and Propagation*, vol. AP-34, no.5, 646, pp. 646–657, 1986.

[5] E. Vilar and J. Haddon, "Measurement and Modeling of Scintillation Intensity to Estimate Turbulence Parameters in an Earth-Space Path," *IEEE Transactions on Antennas and Propagation*, vol. AP-32, no. 4, pp. 340–346, 1984.

[6] T. J. Moulsley and E. Vilar, "Experimental and Theoretical Statistics of Microwave Amplitude Scintillations on Satellite Down-Link," *IEEE Transactions on Antennas and Propagation,* vol. AP-30, no. 6, pp. 1099–1106, 1982.

[7] M. Tamir, E. Azoulay, S. Tsur, and U. Halavee, "Aperture-Averaged Spectral Correlations of Beams in a Turbulent Atmosphere," *Applied Optics*, vol. 23, no. 14, pp. 2359–2362, 1984.

[8] A. D. Wheelon, "Relation of Radio Measurements to the Spectrum of Tropospheric Dielectric Fluctuations," *Journal of Applied Physics*, vol. 28, no. 6, pp. 684–693, 1957.

[9] R. Linfield, "The Effect of Aperture Averaging Upon Tropospheric Delay Fluctuations Seen With a DSN Antenna," *The Telecommunications and Data Acquisition Progress Report 42-124, October–December 1995*, Jet Propulsion Laboratory, Pasadena, California, pp. 1–7, February 15, 1996.
http://tmo.jpl.nasa.gov/tmo/progress_report/42-124/124A.pdf

[10] R. N. Treuhaft and G. E. Lanyi, "The Effects of Dynamic Wet Troposphere on Radio Interferometric Measurements," *Radio Science*, vol. 22, no. 22, pp. 251–265, 1987.

[11] C. Ho and A. Wheelon, "Power Spectrum of Atmospheric Scintillation for the Deep Space Network Goldstone Ka-Band Downlink," *The Interplanetary Network Progress Report*, vol. 42-158, Jet Propulsion Laboratory, Pasadena, California, pp. 1–21, August 15, 2004.
http://ipnpr/progress_report/42-158/158F.pdf

Appendix A
Bessel Functions and Other Integral Equations

The Bessel functions are as follows:

$$\int_0^{2\pi} d\phi \exp\left[r\kappa_r \cos(\phi-\omega)\right] = 2\pi J_0(\kappa_r r) \tag{A-1}$$

$$\int_0^{\infty} J_0(ax)\cos(bx^2)xdx = \frac{1}{2b}\sin\left(\frac{a^2}{4b}\right) \tag{A-2}$$

$$J_0\left(\kappa\sqrt{\rho_1^2+\rho_2^2-2\rho_1\rho_1\cos(\phi_2-\phi_1)}\right) = \sum_0^{\infty}\varepsilon_n J_n(\kappa\rho_1)J_n(\kappa\rho_2)\cos\left[n(\phi_2-\phi_1)\right] \tag{A-3}$$

$$\frac{1}{a^2}\int_0^a xJ_0(x\kappa)dx = \frac{J_1(\kappa a)}{\kappa a} \tag{A-4}$$

The Delta functions are as follows:

$$\int_0^R dx\int_0^R dx' f(x)g(x')\exp\left[i\kappa_x(x-x')\right] = 2\pi\delta(\kappa_x)\int_0^R dx f(x)g(x) \tag{A-5}$$

$$\delta(\kappa\cos\psi) = \frac{1}{\kappa}\delta(\cos\psi) \tag{A-6}$$

$$\int_0^{\pi} d\psi f(\psi)\delta(\kappa\cos\psi) = \frac{1}{\kappa}f\left(\frac{\pi}{2}\right) \tag{A-7}$$

The integral solutions are as follows:

$$\int_0^{\infty}\frac{d\zeta}{\zeta^{11/6}}\left(1-\frac{\sin\zeta}{\zeta}\right) = 0.943 \tag{A-8}$$

$$\int_0^{\infty}\frac{d\zeta}{\zeta^{11/6}}\left[1-\cos\zeta\right] = 1.729 \tag{A-9}$$

$$\int_0^{\infty}\frac{x^{m-1}dx}{1+x^n} = \frac{\pi}{n\sin\left(\frac{m\pi}{n}\right)} \tag{A-10}$$

Appendix B
Antenna Aperture-Averaging Equation

The amplitude fluctuations for a plane wave measured at separated locations can be described by

$$\chi(R) = -2k^2 \int d^3 r A(R,r)\delta n(r) \tag{B-1}$$

$$\begin{aligned}\chi(R+\Delta\boldsymbol{\rho}) &= -2k^2 \int d^3 r A(R+\Delta\boldsymbol{\rho},r)\delta n(r) \\ &= -2k^2 \int d^3 r' A(R,r')\delta n(r'+\Delta\boldsymbol{\rho})\end{aligned} \tag{B-2}$$

where $\boldsymbol{\Delta\rho} = \boldsymbol{\rho}_2 - \boldsymbol{\rho}_1$ is a vector in a plane of a receiver antenna:

$$\langle \chi(R)\chi(R+\Delta\boldsymbol{\rho})\rangle = 4k^4 \int d^3 r A(R,r) \int d^3 r' A(R,r') \langle \delta n(r)\delta n(r'+\Delta\boldsymbol{\rho})\rangle \tag{B-3}$$

where

$$\langle \delta n(r,t)\delta n(r'+\Delta\boldsymbol{\rho},t)\rangle = \int d^3\kappa \Phi_n(\kappa) \exp\left[i\boldsymbol{\kappa}\cdot(\boldsymbol{r}-\boldsymbol{r'}-\Delta\boldsymbol{\rho})\right] \tag{B-4}$$

Thus,

$$\begin{aligned}\langle \chi(R)\chi(R+\Delta\boldsymbol{\rho})\rangle = 4k^4 &\int d^3 r A(R,r)\exp(i\boldsymbol{\kappa}\cdot\boldsymbol{r}) \int d^3 r' A(R,r')\exp(i\boldsymbol{\kappa}\cdot\boldsymbol{r'}) \\ &\times \int d^3\kappa \Phi_n(\kappa)\exp(i\boldsymbol{\kappa}\cdot\Delta\boldsymbol{\rho})\end{aligned} \tag{B-5}$$

The three-dimensional integration on κ is written in spherical coordinates as

$$\int_0^\infty d\kappa^3 \exp(i\boldsymbol{\kappa}\cdot\Delta\boldsymbol{\rho}) = \int_0^\infty \kappa^2 d\kappa \int_0^\pi d\psi \sin\psi \delta(\kappa\cos\psi) \int_0^{2\pi} d\omega \exp(i\boldsymbol{\kappa}\cdot\Delta\boldsymbol{\rho})$$

In the usual case, $\psi = \pi/2$ and $\sin\psi = 1$, so that

$$\int_0^\infty d\kappa^3 \exp(i\boldsymbol{\kappa}\cdot\Delta\boldsymbol{\rho}) = \int_0^\infty \kappa d\kappa \int_0^{2\pi} d\omega \exp(i\boldsymbol{\kappa}\Delta\rho\cos\omega) = 2\pi\int_0^\infty \kappa d\kappa J_0(\kappa\Delta\rho)$$

because

$$4k^4 \int d^3r A(R,r) \exp(i\boldsymbol{\kappa}\cdot\boldsymbol{r}) \int d^3r' A(R,r') \exp(i\boldsymbol{\kappa}\cdot\boldsymbol{r}') = 4\pi^2 k^2 \int_0^H dz \sin\left(\frac{z\kappa^2}{2k}\right)$$

Thus,

$$\langle \chi(R)\chi(R+\Delta\boldsymbol{\rho})\rangle = 4\pi^2 k^2 \int_0^H dz \sin\left(\frac{z\kappa^2}{2k}\right) \int_0^\infty d\kappa\kappa\Phi_n(\kappa) J_0(\kappa\Delta\rho) \tag{B-6}$$

An additional term $J_0(\kappa\Delta\rho)$ that spatially joins together two elements separated by $\Delta\rho$ is included in the spatial covariance. For the antenna aperture averaging, we have

$$\langle \chi(\sigma_1)\chi(\sigma_2)\rangle = 4\pi^2 k^2 \int_0^\infty \kappa d\kappa\Phi_n(\kappa) J_0(\kappa\,|\boldsymbol{\sigma}_1 - \boldsymbol{\sigma}_2|) \int_0^H \sin^2\left(\frac{z\kappa^2}{2k}\right) dz \tag{B-7}$$

where $\boldsymbol{\sigma}_1$ and $\boldsymbol{\sigma}_2$ are, respectively, two elements within the antenna.